

THE PANCHROMATIC HUBBLE ANDROMEDA TREASURY II. TRACING THE INNER M31 HALO WITH BLUE HORIZONTAL BRANCH STARS

BENJAMIN F. WILLIAMS¹, JULIANNE J. DALCANTON¹, ERIC F. BELL², KAROLINE M. GILBERT^{1,3}, PURAGRA GUHATHAKURTA⁴, TOD R. LAUER⁵, ANIL C. SETH⁶, JASON S. KALIRAI⁷, PHILIP ROSENFELD¹, LEO GIRARDI⁸,

Draft version June 5, 2021

ABSTRACT

We attempt to constrain the shape of M31’s inner stellar halo by tracing the surface density of blue horizontal branch (BHB) stars at galactocentric distances ranging from 2 kpc to 35 kpc. Our measurements make use of resolved stellar photometry from a section of the Panchromatic Hubble Andromeda Treasury (PHAT) survey, supplemented by several archival Hubble Space Telescope observations. We find that the ratio of BHB to red giant stars is relatively constant outside of 10 kpc, suggesting that the BHB is as reliable a tracer of the halo population as the red giant branch. In the inner halo, we do not expect BHB stars to be produced by the high metallicity bulge and disk, making BHB stars a good candidate to be a reliable tracer of the stellar halo to much smaller galactocentric distances. If we assume a power-law profile $r^{-\alpha}$ for the 2-D projected surface density BHB distribution, we obtain a high-quality fit with a 2-D power-law index of $\alpha = 2.6^{+0.3}_{-0.2}$ outside of 3 kpc, which flattens to $\alpha < 1.2$ inside of 3 kpc. This slope is consistent with previous measurements but is anchored to a radial baseline that extends much farther inward. Finally, assuming azimuthal symmetry and a constant mass-to-light ratio, the best-fitting profile yields a total halo stellar mass of $2.1^{+1.7}_{-0.4} \times 10^9 M_{\odot}$. These properties are comparable with both simulations of stellar halo formation formed by satellite disruption alone, and with simulations that include some *in situ* formation of halo stars.

Subject headings: galaxies: individual (M31) — galaxies: stellar populations — galaxies: evolution

1. INTRODUCTION

The diffuse envelope of stars that appears to surround most or all Milky Way-mass galaxies (massive galaxies, hereafter) encodes a wealth of information about how such galaxies assembled and developed (e.g. Eggen et al. 1962; Searle & Zinn 1978; Bullock et al. 2001; Bullock & Johnston 2005; Zolotov et al. 2009; Cooper et al. 2010). A major fraction of the stellar mass in such envelopes is expected to be debris from tidally disrupted dwarf galaxies embedded in the dark matter halos. These disrupted galaxies are progressively incorporated into the larger potential well of the main galaxy during its hierarchical, bottom-up assembly. Accordingly, widespread effort has been put into studying massive galaxy halos both observationally and theoretically.

Over the past few decades, major observational progress has been made in our understanding of the build-up of halos through discovery of many dwarf galaxies around the Milky Way (e.g., Ibata et al. 1994; Willman et al. 2005; Belokurov et al. 2007), low surface brightness structures in the Milky Way stellar halo (Ibata et al. 1995; Yanny et al. 2000; Majewski et al. 2003; Bell et al. 2008), and around the

outskirts of many nearby galaxies (e.g., Malin & Hadley 1999; Martínez-Delgado et al. 2008; Bailin et al. 2011; Radburn-Smith et al. 2011), including M31 (e.g., Ibata et al. 2001; Gilbert et al. 2007; McConnachie et al. 2009; Gilbert et al. 2009a). The amount and character of such substructure at $r \gtrsim 10$ kpc is both qualitatively and quantitatively consistent with cosmologically-motivated simulations in which stellar halos are built up through the accretion of dwarf galaxies alone (Bullock & Johnston 2005; Bell et al. 2008; Martínez-Delgado et al. 2010; Xue et al. 2011).

At radii less than ~ 20 kpc, it is expected that some fraction of stellar halo mass may originate in the main potential well (often called *in situ*), either formed early in the formation of the galaxy or kicked up from the disk at later times through tidal interactions (e.g. Kazantzidis et al. 2008; Zolotov et al. 2009; Font et al. 2011; Brook et al. 2012). Studies attempting to disentangle the fraction formed *in situ* 1-2 are challenging both observationally and theoretically for a variety of reasons.

Observationally, the stellar halo has both low surface brightness and relatively low stellar mass, and so is easily overwhelmed by higher surface brightness components of a galaxy, making accurate measurements challenging. A further (related) difficulty is that the separation of a halo from a bulge component (where the bulge in great part is expected to have formed the bulk of its stars in the main galaxy potential well) has been extremely difficult because disk and bulge dominate the stellar halo (Dorman et al. 2012; Courteau et al. 2011, hereafter C11), leading a number of groups to consider both components together (e.g. Irwin et al. 2005; Kalirai et al. 2006; Sarajedini et al. 2012; Font et al. 2011).

¹ Department of Astronomy, Box 351580, University of Washington, Seattle, WA 98195; ben@astro.washington.edu; jd@astro.washington.edu; kgilbert@astro.washington.edu; philrose@astro.washington.edu

² Department of Astronomy, University of Michigan, 550 Church St., Ann Arbor MI 48109; ericbell@umich.edu

³ Hubble Fellow

⁴ UC Santa Cruz; raja@uco.lick.org

⁵ NAOJ; lauer@noao.edu

⁶ University of Utah; aseth@astro.utah.edu

⁷ Space Telescope Science Institute; jkalirai@stsci.edu

⁸ Padova, Italy; lgirardi@pd.astro.it

A related theoretical problem is that in numerical simulations relatively rare modes of star formation at relatively high temperatures and low densities, which are not yet well-characterized, may contribute disproportionately to low-mass diffuse stellar halos (see discussions in Zolotov et al. 2009; Munshi et al. 2012). The correct star formation prescription for the halo gas is still uncertain, making the simulated stellar halo properties less reliable. In what follows, we attempt to give a fresh perspective to this issue by focusing on the possibility of using blue horizontal branch (BHB) stars in M31 as a probe of M31’s inner stellar halo.

1.1. Current M31 Stellar Halo Measurements

Fits to the surface brightness profile of M31 do not constrain the shape of the inner halo. The surface brightness profile is dominated by the red giant branch (RGB) stars in M31. These studies fit all three galaxy components (disk, halo, and bulge) simultaneously, but must assume a halo model inside of ~ 10 kpc where all 3 components contribute significantly. Not only are the fits to the inner halo profile model dependent, the fits by C11 show clear degeneracies between the different components, making extrapolating the halo profile inwards from 10 kpc unreliable. Thus, the modeling of the inner halo can result in significant variations of the stellar halo mass fraction at these inner radii.

Kinematic decompositions of the halo outside of 10 kpc, performed with spectra of individual RGB stars, currently suggest a 2-D projected surface density power-law index of ~ -2 (K. Gilbert et al. ApJ, submitted; Guhathakurta et al. 2005, hereafter G05). However, M31’s bulge and halo are both dynamically hot and exhibit metallicity and/or age gradients (e.g. Kalirai et al. 2006; Gilbert et al. 2007), making it extremely difficult to disentangle M31’s bulge from M31’s halo closer to the galaxy center, even with kinematics of individual red giant branch stars.

Furthermore, a case can be made that it is dangerous to extrapolate the outer halo stellar profiles inwards to small galactocentric distances in M31, or in any other galaxy. Inside of ~ 35 kpc, the stellar populations of the M31 halo are substantially more metal-rich than those of the Milky Way and have a range of ages (Durrell et al. 1994, 2001, 2004; Brown et al. 2006, 2007, 2008; Richardson et al. 2008). In addition, there are deviations from a single power law in the surface brightness profile of the outer stellar envelope of M31 (Kalirai et al. 2006).

Taken together, these differences have led some workers to suggest that at radii $\lesssim 35$ kpc one should think of the extended stellar envelope as an extended bulge instead of halo, or one should simply lump both components together into a spheroid. In addition, simulations of stellar halo formation, both those that are composed only of tidal debris from dwarf disruptions and those that include an *in situ* component, show changes in power law profiles with radius, frequently flattening in profile towards the smallest radii (e.g. Zolotov et al. 2009; Cooper et al. 2010; Font et al. 2011). Without reliable constraints on the shape of the inner halo, comparisons of the observed halo to simulations or estimates the stellar halo mass are hampered.

In short, there are currently no straight-forward tools

for mapping the halo profile in the inner galaxy. Thus any current knowledge about stellar halo profiles is limited to large radii.

1.2. Using BHB Stars to Trace the Halo

Our approach to recovering the inner structure of the halo is to identify a tracer unique to the stellar population of the halo. More specifically, we attempt to define the stellar halo as the population that is responsible for the presence of field blue horizontal branch (BHB) stars. We then check the consistency between our results and previous halo studies. We attempt this new approach in order to avoid the difficulties of more direct kinematic or photometry measurements.

The halo measurements of previous studies have been limited to the outskirts of the galaxy to ensure they are measuring a halo population (e.g. Brown et al. 2008; Richardson et al. 2008; Kalirai et al. 2006). In these regions, previous works have found a total stellar population that is poorly fit with a single power-law profile, motivating a description of the outer parts of M31 in terms of a stellar halo (often taken as synonymous with a power law component), an extended bulge (a Sersic index component prominent out to large radius), and an extended disk (e.g. Ibata et al. 2005; Kalirai et al. 2006, C11).

In contrast to current surface brightness and spectroscopic techniques, the BHB may provide a way to trace the halo profile to small radii, breaking degeneracies between the disk, bulge, and halo galaxy components. The BHB is the part of the horizontal branch just blueward of the RR Lyrae instability strip. It is made of low-mass stars in the phase of central helium burning, with effective temperatures from ~ 7200 – ~ 40000 K. The BHB is routinely subdivided by temperature into three parts, the HBA (~ 7200 K $\lesssim T_{\text{eff}} \lesssim 12000$ K), HBB (12000 K $\lesssim T_{\text{eff}} \lesssim 20000$ K), and EHB ($T_{\text{eff}} \gtrsim 20000$ K) (for a full review on HB evolution see Catelan 2009, and references therein). In this work we include only the HBA, which is the section typically associated with metal-poor populations, when referring to the BHB. For a typical old and metal-poor halo environment, these BHB stars will spend their ~ 100 Myr lifetime confined within a horizontal strip just 0.2 mag wide in M_{bol} , so that the BHB location can be approximated by a simple zero-age horizontal branch (ZAHB) sequence, as the one illustrated in Figure 1.

Although BHB stars are typically associated with low metallicity populations, it is also possible to make hot HB stars at high metallicities. Enhanced mass loss, and possibly high helium content, generate a second formation channel; however this metal-rich channel is more likely to produce extremely hot HB stars, not normal HBA stars, as witnessed by the metal-rich open cluster NGC6791 (e.g. Kalirai et al. 2007), and as demonstrated by the very low formation efficiency of RR Lyrae among metal-rich populations (Layden 1995). BHB stars instead, are likely to have metallicities similar to the RR Lyrae, i.e. with a mean $[\text{Fe}/\text{H}] \sim -1$ (Pietrukowicz et al. 2012) and just a very minor tail of stars extending to high metallicities (see also Figure 5). For this reason, these stars have been successfully used as probes of the Galactic halo stellar population (Preston et al. 1991). As a result, a prominent BHB component is unlikely to be formed by

the higher metallicity disk and bulge populations. We note the possibility of a contribution from the thick disk, which has recently been measured to have a metallicity similar to that of the halo (Collins et al. 2011), but argue against this possibility on the basis of previous M31 disk population studies and kinematic arguments (see § 3.7.2, also Kinman et al. 2009, who find a very low fraction of local BHB stars originating in the thick disk).

There is clearly a BHB component in the M31 stellar halo (van den Bergh 1991), as easily seen in deep HST CMDs in the literature (e.g. Bellazzini et al. 2003; Brown et al. 2003). Furthermore, RR Lyrae stars have been cataloged in M31 far from the central bulge (e.g., Bernard et al. 2012). We note that the BHB stars we are using to probe the halo are distinct from extreme horizontal branch (EHB) stars, which are much hotter than the traditional BHB. These EHB stars are common in metal-rich populations including the M31 (e.g. Rosenfield et al. 2012). and Galactic bulges (e.g. O’Connell 1999; Busso et al. 2005) and therefore would not be appropriate tracers of the halo. Furthermore, EHB stars are quite faint in the optical, as their spectral energy distribution peaks in the far-UV, making them fall below the completeness limit in our ACS data.

Herein we use BHB stars to trace the M31 halo component to small galactocentric distances, where the overall fraction of halo stars is low and difficult to measure any other way. We isolate the BHB in the M31 field population and measure its surface density to galactocentric distances as small as 1.6 kpc from the center of M31. Our measurement of the halo profile provides the means to break degeneracies with other components, as well as to estimate the total halo stellar mass. In § 2 we describe our data set and measurement techniques. In § 3 we present the resulting BHB density profile and argue that it is reasonable to assume that they are all halo members. We then quantify our constraints on the halo profile and compare these to currently-available decomposition measurements and simulations. Finally, in § 5 we provide a brief summary of our results and their place in our understanding of the structure of M31.

We assume a distance of 780 kpc (Stanek & Garnavich 1998) for all conversions from angular distances to kiloparsecs. All power-law indexes refer to 2-D projected surface density profiles. We make no corrections for inclination, as there is no clear evidence in the literature that the M31 stellar halo is non-spherical, we have no way of knowing if an inclination correction is needed. If the halo is indeed significantly flattened and inclined, it would affect the magnitude ranges adopted for our BHB selection in the outer halo fields by ~ 0.1 mag. Such an offset would not significantly impact our surface density measurements; however, flattening would affect our mass estimate, as discussed in § 3.4.

2. DATA ACQUISITION AND ANALYSIS

2.1. *Panchromatic Hubble Andromeda Treasury Data*

As part of the PHAT survey (Dalcanton et al. 2012), we obtained HST/ACS data in F475W and F814W covering a large fraction of the M31 disk. All of the PHAT data for this paper were acquired and analyzed as part of the survey, as detailed in Dalcanton et al. (2012). In short, photometry was performed using the package

DOLPHOT (Dolphin 2000). The output was filtered to reject non-point sources and low-quality measurements, as detailed in Dalcanton et al. (2012). Artificial star tests were performed on each field to allow measurement of completeness as a function of color and magnitude.

In studying the survey photometry, we noticed a blue feature extending across the vertical main-sequence in a few of our survey fields (see Figure 1). Further examination of the areas exhibiting this feature revealed that they all fell within a small corner of the survey, shown in Figure 2. This corner lies at the farthest point that the survey reaches along the M31 minor axis, and thus has the highest ratio of halo to disk stars.

2.1.1. *Counting BHB Stars*

We isolated the BHB component by taking a vertical cut in the CMD at $0.1 < F475W - F814W < 0.5$ (see dashed vertical lines in Figure 1), and plotting F475W and F814W magnitude histograms. Assuming $E_{B-V} = 0.1$, this intrinsic color range ($0.1 < F475W - F814W < 0.5$ after correcting for reddening) corresponds to 7200K–9600K. Our major axis disk field luminosity functions using this color selection was well-fit with a simple straight line, suggesting that the underlying main sequence population has a simple linear luminosity function. We therefore fit these luminosity functions, which clearly contained a significant enhancement at the magnitude expected for the BHB, with a straight line plus a Gaussian; the latter component was then used as a measure of the magnitude and strength of the BHB feature at this color. We chose our color range based on the data in Figure 1. At bluer colors, the BHB sequence extends vertically in our filter set, blending completely with the main sequence. Redward of our BHB selection window, the RR Lyrae instability strip spreads the feature, also making the BHB difficult to isolate. In F814W, we found the peak magnitude to be consistent across all fields where we measured it; however, in F475W, the peak magnitude was slightly less consistent, owing to small amounts of dust reddening. Therefore we show the less dust-affected F814W fits in Figure 3. Finally, we attempted rotated LFs that were orthogonal to the BHB in this color range. We found in these cases the background LF became more complicated as did comparisons across different filter sets. In the end, the simple F814W luminosity function provided the most reliable measurements across our full sample.

The line component of our fits represents the upper main-sequence stars that also occupy this color-magnitude region. The number of BHB stars was obtained by subtracting the line component away from the total, thus removing the upper main-sequence contamination from our BHB sample.

We performed checks to ensure that our sample was not strongly affected by the presence of dust in the M31 disk. First, we checked that the apparent magnitude of the BHB was consistent across all fields. While there was some increased scatter in F475W, it was small (< 0.1 mag), and the scatter was even smaller in F814W (< 0.03 mag). In neither case was a trend with galactocentric distance seen. Furthermore, we inspected the PHAT infrared photometry of all of the regions where we detected the BHB, and found the red giant branch to have a single, narrow tip in all regions. We also checked the reddening value for the nearest globular cluster to the region,

which is very low (B201; $E_{(B-V)}=0.04\pm 0.02$; Fan et al. 2008). Finally, we inspected the *Spitzer* 24μ maps of the regions, finding no significant emission above the background. Therefore, with all of these tracers, there is no evidence for the presence of a significant dust layer at these radii along the minor axis that would affect our measurements of the BHB.

2.1.2. BHB Upper Limits

Outside of 2.5 kpc on the minor axis and 5 kpc on the major axis, artificial star tests show that our 50% completeness limit is a magnitude or more below the BHB feature, making it simple to isolate and measure the BHB component. In contrast, we were not able to isolate the feature inside of 2.5 kpc on the minor axis and 5 kpc on the major axis, because our photometric uncertainties and completeness affected our data too strongly at the magnitudes of interest. Attempts to solve this problem by applying completeness corrections from false star tests were not effective, due to the sharp cutoff in completeness in our region of interest. Essentially, when completeness corrections become greater than a factor of 2, the inferred number of stars has associated uncertainties that our fitting routine could not overcome. Therefore, at these inner radii, we assume that the BHB is located in the same color-magnitude range as in all of the fields where it was measured directly ($25.1 < F814W < 25.3$ and $0.1 < F475W - F814W < 0.5$). We then counted the total number of stars in this range and corrected for the mean completeness. This calculation gives us the total number of stars which potentially could be BHB stars. However, because we cannot reliably subtract off the contribution from the MS or post-AGB stars, we quote our measurements in these fields as upper limits.

Our interpretation of the inner radius measurements as upper limits is unaffected by magnitude biases from crowding. In very crowded fields, such as the inner M31 bulge, our photometry shows biasing towards brighter magnitudes. Such biasing would put the BHB stars brightward of the magnitude range within which we are counting BHB stars. Because the luminosity function increases toward fainter magnitudes, measuring the completeness-corrected numbers of stars at a brighter magnitude interval (to take such biasing into account) would only serve to *lower* our upper limits, making them less conservative. In one case, our completeness-corrected LF showed a small peak at $F814W=25.05$, slightly brightward of our assumed BHB magnitude. We verified that shifting our window 0.1 mag brightward ($25.0 < F814W < 25.2$) to include this small peak did not significantly impact our results. Such a change only slightly shifted our upper-limits, and the lowest upper limit changed by $< 3\%$. Thus our upper limits are conservative and are not strongly sensitive to the precise magnitude cuts.

We attempted to augment our radial baseline by applying the same measurement techniques to other fields. We first attempted to detect the BHB in the PHAT survey data along the major axis. However, we were unable to isolate a BHB feature because the expected number of BHB stars from the halo is small compared to the number of main-sequence stars present in the disk component along the major axis. These fields had such high contamination levels that upper-limits measured using our blind

counting technique were so large that they proved to be of no use. We therefore do not report any measurements taken near the major axis.

2.2. Relevant Archival Data

In order to greatly increase our radial baseline, we searched for relevant archival data that would contain resolved photometry of the BHB in the M31 halo. First, we found the deep photometry of the halo released as high level science products (PIDs: 9453, 10265, 10816, PI: Brown, Brown et al. 2009, 2008, hereafter B08). Then we found deep archival imaging away from the major axis or known streams that we could quickly process with the PHAT pipeline (PID: 10394, PI: Tanvir, Tanvir et al. 2012; PID: 11362, PI: Rich)

2.2.1. Public Deep Halo Photometry

We downloaded the very deep photometry catalogs of B08, from ACS fields at 11, 21, and 35 kpc out along the minor axis, as well as one located at $R=20$ kpc in a known stream. These fields are well away from the disk, contain stars at the location of the BHB, and have no main-sequence stars.

For these data, which use a different filter set and different photometric system, we found that the feature was isolated enough that a comparable measure of the number of BHB stars (leaving out the instability strip and the vertical extension) was obtained from counting all stars with $-1.0 < F606W_{STMAG} - F814W_{STMAG} < -0.6$ and $26.0 < F814W_{STMAG} < 26.7$. The difference in $F814W$ magnitude corresponds simply to the difference in $F814W$ zeropoint between VEGAMAG (25.5) and STMAG (26.8). The color range was chosen by looking at the CMDs to find the color corresponding to the BHB feature; however, it is similar to the expected shift of ~ -1 (a formal transformation of $F475W - F814W = 0.3$ results in $F606W_{STMAG} - F814W_{STMAG} = -0.7$).

Although some of these fields are known to lie in streams, the fraction of stream stars is well-constrained by kinematics (Gilbert et al. 2009b). For the 11 kpc field and 20 kpc stream field, only $56\pm 16\%$ and $25\pm 10\%$ of the stars belong to the kinematically hot halo (Gilbert et al. 2009b). These fractions are determined by spectroscopy of RGB stars in fields that overlap the HST imaging. The kinematics of stars in these fields display distinct cold streams with low dispersion as well as a population of stars with high dispersion (hot) halo component; maximum-likelihood fits to the line-of-sight velocity distributions in each field yield estimates of the fractions of stars in the hot and cold components. While both of these fields are in known streams, the outer field lies on a more overdense stream, resulting in a lower fraction of hot halo stars. Therefore, we scale our measurements in these fields by 0.56 and 0.25 respectively, to account for the overdensities, and we include the associated errors in our uncertainties. We note that accounting for these overdensities is necessary because of the small sample area of the ACS field of view at the distance of M31, as well as the bias of HST programs to point at streams. Larger areas in random halo locations, as one would obtain in more distant systems, would include both overdense and underdense regions, averaging out to the true mean density of the halo. In addition, there is some

chance that the streams and the rest of the halo have different BHB properties in M31, as has been seen in the Galaxy (e.g. Bell et al. 2010); however, the similar F_{BHB} values seen through the streams and halo (see Figure 4) suggests that, if such differences are present in M31, they do not significantly affect our study.

2.2.2. Other Relevant Archival Observations

We searched for other archival ACS observations suitable for our project. Although there have been many ACS observations in the M31 halo, most were either located on known overdense streams or were too close to the major axis to provide a clean measurement of the BHB. Unlike the B08 fields, other archival stream fields did not have spectroscopically determined stream fractions. Therefore we only included fields outside of known streams.

We found 2 fields with favorable locations and depth. These were a parallel observation in program 11632, which was looking at background QSOs (we refer to this field as 11632_M31-HALO-SE), and an observation of a halo globular cluster (we refer to this field as 10394_M31-HALO-NW). For this latter field, a $20'' \times 20''$ region centered on the globular cluster we exclude from our analysis.

These 2 fields were taken in F606W and F814W like the B08 fields; however, we reduced them in our own pipeline using a stricter quality cut appropriate for less crowded fields. In crowded fields, the crowding parameter is high for most of the stars because they all have close neighbors. In sparse fields, crowding is very sensitive to background galaxies because shredded background galaxies have photometry similar to crowded stars. This contaminant is insignificant in crowding-limited fields with hundreds of thousands of real stars, but is significant in sparse fields with tens of thousands of real stars. Much cleaner CMD features (such as the BHB) are gained by limiting the crowding cut in sparse fields. We produce CMDs similar in quality to those of B08 at the BHB by applying a crowding cut of 0.1 to these halo fields. Our artificial star tests showed that even with this more conservative cut, we are complete at the location of the BHB in these sparse fields.

3. RESULTS

3.1. BHB Magnitude

Our measurements of the BHB feature are detailed in Table 1. These include, for each ACS field, the median (projected) galactocentric distance of the stars from the center of M31, the apparent magnitude of the BHB peak in our color range, the number of BHB stars, the number of RGB stars in our selection region, and the resulting BHB/RGB fraction. The measurements are plotted in Figures 3–4. We find that the feature has an apparent magnitude of $F814W = 25.23 \pm 0.03$, at a $F475W - F814W$ color of 0.3. Assuming a distance modulus of 24.47 (Stanek & Garnavich 1998) and foreground extinction of $A_V = 0.21$ (Schlegel et al. 1998), this corresponds to $M_{F814W} = 0.63 \pm 0.05$. The magnitude and color are consistent with the model BHB shown in Figure 1, which has $[Fe/H] = -1.7$; however, all model BHBs with $-2.3 < [Fe/H] < -1.0$ are similar to our observed BHB.

3.2. BHB/RGB Fraction

There is also information contained in the relative number of stars in the BHB feature compared to more well-populated features. For example, since BHB stars are typically produced by low metallicity populations, there may be a relation between the fraction of BHB stars present in an old population and the population’s metallicity. To assess the relative strength of the BHB feature in our data, we calculated the ratio of the number of stars in the Gaussian component of the histogram fit (N_{BHB}) to the number of stars with $22.0 < F814W < 22.5$ and $1.5 < F475W - F814W < 3.5$ (N_{RGB}). We took the RGB sample from $23.8 < F814W_{STMAG} < 23.3$ in the B08 data. This magnitude slice provides a good proxy to the total stellar mass in the field, as it is dominated by the very well populated RGB. We tailored the magnitude range to yield a fraction ($F_{BHB} \equiv N_{BHB}/N_{RGB}$) close to unity for ~ 12 Gyr old clusters with $[Fe/H] \sim -1$. These values allow for easy comparisons between the halo light fraction and F_{BHB} (see § 3.5)

Once we had defined F_{BHB} to measure the strength of the BHB in our data, we checked its sensitivity to population metallicity by measuring it for a large sample of well-studied globular clusters. This comparison was performed to look for similarity between the M31 halo and Galactic globular clusters of similar age and metallicity. Since the Galactic halo, and most of the globular clusters, significantly differ in age and metallicity from the M31 halo, only the higher metallicity and somewhat younger end of the globular clusters is directly comparable. However, we include the full ACS globular cluster treasury program (Sarajedini et al. 2007; Dotter et al. 2010) for context.

Specifically, we measured the BHB fractions of the Galactic globular clusters (GCs) of the ACS globular cluster treasury program (Sarajedini et al. 2007; Dotter et al. 2010). All GC CMDs were corrected for their different distances and extinctions using the values from Dotter et al. (2010). Values for metallicity and age for NGC 6388 were taken from Worley & Cottrell (2010) and for NGC 6441 from Gratton et al. (2006). Distances and reddening values for these two clusters were taken from Harris (1996). We then took our BHB from the CMD region with $-0.1 < M_V - M_I < 0.3$ and $-0.3 < M_I < 0.8$, and our RGB from the CMD region with $-2.0 < M_I < -1.5$. The results are shown in Figure 5. Applying the mean metallicities and ages from the full-field CMD analysis of B08, we find that the BHB fraction of the M31 halo is in good agreement with the $F_{BHB} - [Fe/H]$ correlation for Galactic GCs, despite the broad metallicity spread contained in the M31 fields.⁹ F_{BHB} values for the M31 halo (~ 0.7) are similar to those measured for GCs of similar ages (11 Gyr) and metallicities ($-1.0 - -0.5$). Furthermore, we note that F_{BHB} is the same in fields inside and outside of streams, suggesting that the streams have similar F_{BHB} to the kinematically hot halo. This finding is consistent with the full-field analyses of B08, which found the ages and metallicities of the stream field to be similar to other halo fields.

Figure 5 confirms that at old ($\gtrsim 10$ Gyr) ages strong BHB populations are associated with low metallicities.

⁹ Although the B08 metallicities are not from spectroscopy, they are in agreement with spectroscopic metallicity measurements of stars in the vicinity.

Below $[\text{Fe}/\text{H}] < -1.5$, we find F_{BHB} is universally high ($1 < F_{\text{BHB}} < 6$) with a median of 3.2. At higher metallicities, the strength of the BHB population drops dramatically, falling by a factor of 10 as the metallicity rises to $[\text{Fe}/\text{H}] < -0.5$. Above this metallicity, the BHB is unlikely to exist at all. Finally, we note that this comparison includes the moderately metal-rich globular clusters NGC 6388, NGC 6441, and Lynga 7, which exhibit blue horizontal branches, showing that these clusters do not significantly affect the overall behavior of F_{BHB} with age and metallicity.

We can use the data in Figure 5 to place limits on the metallicity distribution of the M31 stellar halo. If we assume that all of the BHB stars come from a metal-poor tail in the population and that the outer fields from the archive are pure M31 halo, we can infer from Figure 5 that no more than $\sim 10\%$ of the halo population is likely to belong to a metal-poor than with $[\text{Fe}/\text{H}] < -1.5$. Such a tail would produce F_{BHB} values higher by a factor of 2 in these pure halo fields. This result is also consistent with the full CMD analyses summarized in B08, which have little stellar mass at $[\text{Fe}/\text{H}] < -1.5$. We note that this result relies on the assumption that F_{BHB} behaves in a similar way in M31 and the Galaxy. Figure 5 is consistent with such an assumption; however, there have been studies that suggest otherwise (e.g. Rich et al. 2005).

Finally, Figure 5 shows us that the youngest (and most metal-rich) halo field appears to have a somewhat high F_{BHB} value for its metallicity, making it consistent with the values from the other fields. Thus, our measurements suggest that the F_{BHB} value in the halo is relatively independent of radius. Therefore, if the halo indeed has a gradient in its mean metallicity, as has been suggested in several works (e.g. Kalirai et al. 2006; Brown et al. 2008), then the gradient does not appear to strongly affect F_{BHB} in the radial range considered here. This result is consistent with the fact that the BHB surface density measurements obey a single-sloped power-law profile from 3–35 kpc in Figure 4.

3.3. BHB Surface Density Profile

We now analyze the surface density profile of BHB stars. If the stellar halo can be defined as the population that is responsible for the field BHB stars, then this profile should be consistent with previous measurements of the outer halo. We show our measurement of the surface density profile of BHB stars in M31 in the left panel of Figure 4. The surface density falls off with galactocentric distance following roughly the surface brightness profile of the halo measured by G05 and C11 outside of 11 kpc. However, the BHB profile is steeper between 3 kpc and 11 kpc than inward extrapolations of such current halo models. Interestingly, our data suggest a single power-law slope all the way from 3 kpc to 35 kpc. The slope is steeper than (but within the uncertainties of) G05, and it is similar in slope to the outer halo portion of the fits of C11. Thus, our data are providing a new constraint on the shape of the inner halo, suggesting the single power-law slope extends inward to 3 kpc before flattening.

We fit to the BHB surface density profile using the halo parametrization of C11. When fitting the data, we only applied our lowest measured upper limit by setting the value and uncertainty both equal to half of the up-

per limit. The power-law function from C11 provides an excellent fit to the BHB data ($\chi^2_{\nu} = 0.97$).

$$\Sigma(r) = \Sigma_* \left[\frac{(1 + R_*/a_h)^2}{(1 + r/a_h)^2} \right]^{\alpha/2}$$

Where $\Sigma(r)$ is the BHB surface density at radius r , α is the projected 2D spatial density distribution power-law index, and a_h is a core radius (in units of kpc) inside of which the profile flattens. Σ_* and R_* are normalization constants. Not surprisingly, the best fit has the surface density right at our lowest upper limit. Our data constrain the model to $\alpha = 2.6^{+0.3}_{-0.2}$ and $a_h = 2.7^{+1.0}_{-0.8}$ kpc. While this functional form features a core and a central slope that goes to zero as $r \rightarrow 0$, we do not claim the actual detection of a core in the inner halo, only that the slope decreases to < 1.2 interior to 3 kpc (a steeper profile would exceed our upper limit at 1.6 kpc). We only use this functional form to aid in comparison with previous measurements.

How do our halo parameters compare with other measurements? We first compare with other estimates of power law slopes. C11's surface brightness decomposition study gives a power law index of $\alpha = 2.52 \pm 0.08$, in excellent agreement with our power law. G05 finds $\alpha = \sim -2$ with no quantitative uncertainties, and thus roughly consistent with our result. A more formal result from a spectroscopically confirmed sample of M31 halo stars yields $\alpha = 2.2 \pm 0.2$ (K. Gilbert et al., ApJ, submitted), also consistent with our measurement. We have also estimated a flattening radius for the BHB profile (a robust measurement), which as long as the BHB/RGB ratio for the halo is constant (an assumption) is consistent with a core radius for the stellar halo as a whole. Our estimate does not agree with others in the literature (C11 have a large core, attributing instead much of that light to the disk component; and G05 lack a core at all in their parametrized profile), but the constraints from other works were necessarily weak due to the small fraction of halo stars at these small radii.

3.4. The Mass of M31's Stellar Halo

We can integrate our 2-D projected surface density profile to obtain an estimate of the total halo stellar mass. First, we make the strong assumption that the BHB surface density is directly proportional to the halo stellar mass surface density, effectively making $\Sigma(r)$ the profile of the stellar halo surface density. Taking $\mu_V = 29$ mag arcsec $^{-2}$ at 21 kpc (from integrating the 21 kpc field catalog of B08), $M_{V_{\odot}} = 4.82$ and assuming a stellar mass to V-band light ratio of 1.5 (Bellazzini et al. 2012), we calculate $\Sigma_* = 1.4 \times 10^5 M_{\odot} \text{ kpc}^{-2}$ and $R_* = 21$ kpc.

Then, we assume azimuthal symmetry, making the total mass equal to the following integral:

$$M_{\text{tot}} = \int \Sigma(r) dA = \int_0^{2\pi} \int_0^{260} r \Sigma(r) dr d\theta$$

This calculation yields a total halo stellar mass out to the virial radius (260 kpc Seigar et al. 2008) of $2.1^{+1.7}_{-0.4} \times 10^9 M_{\odot}$, with a half-mass radius of 7 kpc. Changing the outer boundary of the integration has a small effect on the resulting value. Integrating to

40 kpc (near the outer boundary of our photometry data) yields $1.8 \times 10^9 M_\odot$, while integrating to infinity yields $2.3 \times 10^9 M_\odot$. We also note that many other stellar halos/envelopes appear to be oblate within 10 – 20 kpc with axis ratios c/a between 0.4 and 0.7 (e.g., the Milky Way: Jurić et al. 2008; NGC 253: Bailin et al. 2011; M81: Barker et al. 2009, M. Vlahić et al. in prep.; NGC 2403: Barker et al. 2012), it is possible that our assumption of azimuthal symmetry will turn out to be incorrect. In that case, we expect that the stellar mass estimate would scale very approximately as a/c (the inverse of the projected axis ratio of the stellar halo). This simple scaling applies to the idealized case, where the M31 minor axis is aligned with that of the minor axis of the spheroid and there are no projection effects.

3.4.1. Comparing with Other Stellar Halo Measurements

Comparing with previous estimates of M31’s halo mass, our measurement is slightly on the high side, but broadly consistent with expectations. We note that our estimate is less than an inward extrapolation of the power-law (index = 2.2 ± 0.2) of Gilbert et al. (ApJ, submitted), or other similar results (e.g. index = 2.17 ± 0.15 , Tanaka et al. 2010; index = 1.91 ± 0.11 , Ibata et al. 2007; index ~ 2.3 , Irwin et al. 2005) which results in a halo stellar mass (assuming no core and excluding the cusp inside of 1 parsec) of $\sim 1.3 \times 10^{10} M_\odot$ out to the virial radius and a half-mass radius of < 1 kpc. If we apply the a_h value measured from the BHB profile to the Gilbert et al. (ApJ, submitted) profile, the resulting halo stellar mass will be the consistent with our value ($1.8 \times 10^9 M_\odot$, but with a half-mass radius of ~ 16 kpc). Assuming $M/L \sim 2$, the measurement of Ibata et al. (2007) yields $\sim 2 \times 10^9 M_\odot$. Irwin et al. (2005) estimate $\sim 2.5\%$ of the total light from M31 is from the halo, and C11 estimates 4%. Assuming a total M31 luminosity of $2 \times 10^{10} L_{B\odot}$ and $M/L_B \sim 2$, these correspond to stellar halo masses of $1.0 - 1.6 \times 10^9 M_\odot$, respectively.

We can also compare our M31 stellar halo mass with those of other nearby large disk galaxies. Our estimate of the stellar mass of the halo of M31 is less than current estimates for the mass of the stellar halo of the nearby disk galaxy NGC 253 ($4 \times 10^9 M_\odot$ Bailin et al. 2011), but larger than current estimates for the mass of the stellar halo of the Milky Way out to 40 kpc ($3.7 \pm 1.2 \times 10^8 M_\odot$, Bell et al. 2008; $2 - 10 \times 10^8 M_\odot$, Siegel et al. 2002; Jurić et al. 2008; Deason et al. 2011).

3.4.2. Comparing with Simulations

M31 and the Milky Way live in massive dark matter halos of similar mass ($1.4 \times 10^{12} M_\odot$ Watkins et al. 2010). The stellar mass of the Milky Way disk is estimated to be $5.5 \times 10^{10} M_\odot$ (Flynn et al. 2006), and that of M31 is estimated to be roughly the same when determined from the absolute visual magnitude of $M_V \sim -21.0$ (Font et al. 2011). Thus, simulations of Milky Way-like galaxies can be compared to M31 observations as well as Milky Way observations.

Comparing to cosmologically-motivated simulations in which the stellar halo is built up through the accretion of dwarf galaxies alone, we find a reasonable degree of agreement between the properties we infer for M31’s stellar halo and BJ05 and C10. BJ05 find halo stel-

lar masses $\sim 2 \times 10^9 M_\odot$, with 3-D power law slopes outside 10kpc of between -2.5 and -3.5 . C10 find a somewhat wider range in possible halo masses, between $10^8 M_\odot$ and $2.5 \times 10^9 M_\odot$, and 3-D power law slopes ranging between -2 and -4.5 . Hydrodynamical models of stellar halo formation that include an *in situ* component find rather higher stellar masses, $0.5 - 3.4 \times 10^{10} M_\odot$ (Zolotov et al. 2009)¹⁰. Possibly relevant given the strong evidence of a very active M31 merger history (e.g. Gilbert et al. 2009a; McConnachie et al. 2009) is that both Zolotov et al. (2009) and Font et al. (2011) find that the galaxies with the most active merger histories have the lowest *in situ* fractions in their simulations. Yet, simulated stellar halos have large halo-to-halo scatter which is merger history-dependent; given this scatter, we conclude at this stage that the properties of M31’s stellar halo appear to be consistent with the range of stellar halos expected in a cosmological context.

3.5. BHB/RGB Ratio Profile

We can use the data in the right panel of Figure 4 to assess the fraction of halo stars at small radii. In the right panel of Figure 4, we plot F_{BHB} as a function of galactocentric distance, along with the G05 and C11 models of the fraction of total light coming from the M31 halo. The models suggest that the relative strength of the halo clearly increases with galactocentric distance out to 11 kpc, then remains relatively constant at the pure halo value. This radial distribution suggests that the population becomes dominated by halo members outside of ~ 11 kpc.

The behavior of F_{BHB} in Figure 4 is consistent with what we expect for a halo population based on the G05 and C11 models. At large radii, the measured values of F_{BHB} are consistent with being flat (although the uncertainties are large, due to the small number of stars). At smaller radii, however, the strength of the BHB feature falls dramatically compared to the RGB. Empirically, this drop indicates the increasing contribution of old stellar populations that do not host BHB stars. If F_{BHB} for the M31 halo is roughly constant with galactocentric distance, then the low values inside of 11 kpc are due to the increased RGB contribution from the bulge and disk components. If we assume that the BHB stars are all halo members and that F_{BHB} for the halo is 0.7, then the expected behavior of F_{BHB} is to follow $0.7H/T$ where H is the halo stellar surface density and T is total stellar surface density.

Perhaps not surprisingly, both the radial distribution of F_{BHB} and the number density profile suggest that the BHB stars inside of 4.5 kpc do not fit inward extrapolations of current models of the halo profile. Inside of 5 kpc, F_{BHB} is significantly larger than expected. This excess in BHB stars suggests a number of possibilities, which we have explored, or address in the subsections that follow. 1) The halo has a different shape from inward extrapolations of current decompositions (the interpretation we explored in sections 3.3 and 3.4). 2) F_{BHB} of the halo is not constant. 3) The bulge is contaminating the BHB sample. 4) The disk is contaminating the BHB sample. We now discuss these latter 3 possibilities and argue that

¹⁰ Font et al. (2011) do not quote stellar halo masses as all the properties quoted in their work are for bulge+halo.

they are unlikely, leaving us to conclude that we have indeed identified a means by which to constrain the shape of the inner stellar halo.

3.6. Does the Halo Produce BHB Stars at all Radii?

An assumption involved in our analysis is that the M31 stellar halo produces field BHB stars in the same fraction at all radii. While our results from 10–35 kpc suggest that this assumption is reasonable, there is no clear way to test the assumption at small radii. Indeed, our upper-limits inside of 2 kpc allow the possibility that there is no population that produces a field BHB at these small radii. We stress that our profile only describes the population that produces a field BHB, which we suggest *may be* a reasonable way to define the M31 stellar halo. Thus, in this analysis, all kinematically hot stars beyond those required to produce the BHB profile shape (i.e. many of the stars inside of 3 kpc) are associated with the M31 bulge.

Even if the halo produces Field BHB stars at all radii, F_{BHB} of the halo component may not be constant. The outer M31 halo (outside of ~ 10 kpc) is known to have a metallicity gradient (Kalirai et al. 2006). However, this gradient is *negative* (metallicity increases with decreasing radius). While it is known that the *total* HB fraction (including the RHB) increases with increasing metallicity (Salaris et al. 2004), based on the behavior of F_{BHB} in Figure 4, F_{BHB} decreases with increasing metallicity. Thus, we would expect the *stellar halo only* F_{BHB} to decrease slightly toward the galaxy center. Such behavior would make F_{BHB} *even lower* than the dashed or dotted curves in Figure 4 near the center, which is the opposite of the observed behavior. Therefore, a changing F_{BHB} of a halo of the type currently in the literature appears an unlikely explanation for the observed radial profile. We note that if the halo F_{BHB} does decrease towards smaller radii, the stellar mass and power law slopes of the halo inferred in sections 3.3 and 3.4 would increase. We now move on to discuss the possibility of bulge or disk contamination.

3.7. Are the BHB Stars From the Stellar Halo?

An important assumption involved in our use of the BHB as a probe of the M31 stellar halo is that neither the bulge nor the disk components contribute significantly to the field BHB. Here we argue that our data suggest this assumption is reasonable. As detailed below, if we assume that a significant fraction of BHB stars belongs to either the bulge or the disk, we can fit the profile, but only if these components contain old, metal-poor populations that have not been observed any other way. Furthermore, the density of BHB stars from 3–35 kpc appears to follow a single power-law distribution. Thus, the BHB stars appear to belong to the stellar halo, which extends to small radii with a slightly different structure than inward extrapolations of currently-available decomposition models. Inside of ~ 3 kpc, simple inward extrapolations greatly overpredict the observed numbers of BHB stars, suggesting a break in the profile.

3.7.1. Possible Contributions of Bulge BHB stars

One possible source of excess BHB stars at small galactocentric distances is the bulge. However, given the

degree to which the bulge dominates at small radii, the low numbers of BHB stars in M31 seen inside of 2 kpc suggests that the bulge population is not responsible for the excess. Furthermore, the high-metallicity of the bulge ($0.0 \lesssim [\text{Fe}/\text{H}] \lesssim 0.4$ out to 1 kpc, Saglia et al. 2010) also argues against it as the source of the BHB stars seen at 2.7–4.5 kpc. On the other hand, the bulge is known to contain a broad range of metallicities (Sarajedini & Jablonka 2005). If we assume that some fraction of the bulge population is metal-poor enough to produce a significant BHB ($[\text{Fe}/\text{H}] < -0.5$), then we can estimate what fraction of metal-poor stars would best reproduce the BHB profile. If the resulting estimate is reasonable, then our assumption that the BHB traces the halo becomes questionable.

The potential contribution of the bulge to the BHB is different depending on the M31 bulge profile. Therefore we tested both the bulge profiles of C11 and G05, which bracket the possibilities of halo size. The C11 bulge is small, and the G05 bulge is large.

First, assuming the decomposition models of C11, we can calculate the bulge properties necessary to reproduce the observed BHB density profile. The preferred C11 fit has a small bulge component that decreases very steeply to zero by a minor axis distance of 4.5 kpc. Given this decomposition fit, it is impossible for the bulge to be responsible for the BHB stars because there would not be enough stellar mass associated with the bulge at 3–5 kpc to produce the observed number of BHB stars, even if the bulge metallicity were as low as the halo metallicity.

If instead we assume the decomposition model of G05 (large bulge), we can produce a BHB profile consistent with the observations if the bulge has a steep increase in the fraction of metal-poor stars outside of 1 kpc. If we assume that some fraction of the bulge population is metal-poor enough to produce a BHB ($[\text{Fe}/\text{H}] < -0.5$), we can estimate what fraction of metal-poor stars would best reproduce the BHB profile. Our very conservative upper-limits at these radii (1.6 kpc) suggest that less than 10% of the inner bulge population is metal-poor enough to produce a BHB. We can bring the profiles in complete agreement by imposing a fraction of metal-poor stars in the M31 bulge that increases *very* steeply, from 0% to 50% from the galaxy center to 2.5 kpc. Another way to bring the profiles into agreement would be to decrease the metallicity of the metal-poor component of the bulge. This explanation is possible, but it is not likely, as it would be odd if the metal-poor stars of the bulge were of lower metallicity than those of the halo. Since no such steep metallicity gradient has been observed at these radii in the bulge, it appears unlikely that the BHB stars at 2.7–4.5 kpc are dominated by the bulge component.

3.7.2. Possible Contributions of Disk BHB stars

Another possible source of excess BHB stars is the outer disk component. However, there is a very powerful empirical argument against disk stars being responsible for the prominent BHB population at 2.7–4.5 kpc along the minor axis: the BHB is not detected in the outer fields along the *major axis* of the PHAT survey data, as would be expected if the disk stellar populations are well-mixed (as an old population like the BHB is expected to be). The deprojected disk radius of 2.7–4.5 kpc is 1–1.5 degrees. The PHAT data only extend to ~ 1 degree along

the major axis, but the B08 disk field (~ 2 degrees out on the major axis) shows very little evidence for the old (>10 Gyr), metal-poor component (Brown et al. 2006) needed to produce a BHB excess. Therefore it appears that the disk is unlikely to be a significant source of BHB stars. It is worth noting that this lack of BHB stars is not necessarily because the metallicity of the outer disk isn't low enough, but rather may indicate that the vast majority of outer disk stars are too young to produce a prominent BHB. Furthermore, kinematic measurements suggest a low disk contribution at these minor axis radii (Gilbert et al. 2007, $\lesssim 10\%$ at 9 kpc). Thus, both the observed populations of the disk itself and the spectroscopic disk fraction argue against a disk origin of the BHB stars at these radii.

4. CONCLUSIONS

We have measured the number density of BHB stars in M31 at galactocentric distances ranging from 1.6 kpc to 35 kpc using photometry from the PHAT survey along with archival halo ACS fields. Our measurements show that the properties of the BHB of M31 are consistent across two degrees of galactocentric distance. Galactic globular clusters with ages of ~ 10 Gyr and metallicities of $-1.0 \lesssim [\text{Fe}/\text{H}] \lesssim -0.5$ (similar to those of the M31 halo values measured from deep CMD analysis) have BHB properties that match the M31 halo as well. Taken together, these measurements suggest the BHB is a useful tool for tracing galaxy halos.

In additional tests, we showed that the BHB surface density profile follows that of the known halo outside of 10 kpc. However, there is an excess of BHB stars at 2.7–4.5 kpc over inward extrapolations of current M31 halo profiles. To match the radial profile of the BHB a combination of halo and bulge and/or disk components can be applied; however, the contributions of these components that is required is inconsistent with the expected properties of the M31 bulge and disk populations at these radii. While it is possible that the disk and/or bulge populations could be contaminating our BHB sample, there is no compelling evidence that the M31 bulge or

disk harbors a significant BHB population at any radius. Furthermore, these components would need to be contributing BHB stars in just the right proportions for the BHB density to follow a power-law density distribution. Such a conspiracy is not impossible, but seems unlikely. Thus, our use of the BHB to trace the inner halo is further justified.

The BHB data are well matched by a power-law with an index of $2.6_{-0.2}^{+0.3}$ outside of 3 kpc decreasing to <1.2 inside of 3 kpc. This profile describes the population that produces a field BHB, which we suggest is a reasonable way to define the M31 stellar halo. In this picture, all kinematically hot stars that do not follow this profile could be associated with the M31 bulge. Our profile slope is consistent with the range in slopes characteristic of simulations of stellar halo formation in a cosmological context.

Normalizing our best-fitting profile function to a halo stellar mass density of $1.4 \times 10^5 M_{\odot} \text{ kpc}^{-2}$ at 21 kpc yields a total stellar halo mass of $2.1_{-0.4}^{+1.7} \times 10^9 M_{\odot}$ for M31. This mass compares well with, but is on the high side of, other estimates of the M31 halo stellar mass, and it is significantly higher than current estimates of the stellar halo mass of the Milky Way.

About a decade ago, the first large stream in M31 was discovered (Ibata et al. 2001). Since then, the M31 halo has been mapped to large radii with Keck (K. Gilbert et al., ApJ, submitted) and the CFHT (McConnachie et al. 2009), and all measurements show significant structure on small scales indicative of a very rich merger history. The BHB stars of the halo as measured with HST appear to paint the same picture. The shape and mass of the stellar halo as measured with BHB stars are broadly consistent with those of simulated halos that contain a significant fraction of accreted stars.

Support for this work was provided by NASA through grants GO-12055 and through Hubble Fellowship grants 51273.01 awarded to K.M.G. from the Space Telescope Science Institute, which is operated by the Association of Universities for Research in Astronomy, Incorporated, under NASA contract NAS5-26555.

REFERENCES

- Bailin, J., Bell, E. F., Chappell, S. N., Radburn-Smith, D. J., & de Jong, R. S. 2011, ApJ, 736, 24
- Barker, M. K., Ferguson, A. M. N., Irwin, M., Arimoto, N., & Jablonka, P. 2009, AJ, 138, 1469
- Barker, M. K., Ferguson, A. M. N., Irwin, M. J., Arimoto, N., & Jablonka, P. 2012, MNRAS, 419, 1489
- Bell, E. F., Xue, X. X., Rix, H.-W., Ruhland, C., & Hogg, D. W. 2010, AJ, 140, 1850
- Bell, E. F., et al. 2008, ApJ, 680, 295
- Bellazzini, M., Cacciari, C., Federici, L., Fusi Pecci, F., & Rich, M. 2003, A&A, 405, 867
- Bellazzini, M., Dalessandro, E., Sollima, A., & Ibata, R. 2012, MNRAS, 423, 844
- Belokurov, V., et al. 2007, ApJ, 654, 897
- Bernard, E. J., et al. 2012, MNRAS, 420, 2625
- Brook, C. B., et al. 2012, ArXiv:astro-ph/1206.0740
- Brown, T. M., et al. 2008, ApJ, 685, L121
- Brown, T. M., Ferguson, H. C., Smith, E., Kimble, R. A., Sweigart, A. V., Renzini, A., Rich, R. M., & Vandenberg, D. A. 2003, ApJ, 592, L17
- Brown, T. M., et al. 2009, ApJS, 184, 152
- Brown, T. M., et al. 2007, ApJ, 658, L95
- Brown, T. M., Smith, E., Ferguson, H. C., Rich, R. M., Guhathakurta, P., Renzini, A., Sweigart, A. V., & Kimble, R. A. 2006, ApJ, 652, 323
- Bullock, J. S., & Johnston, K. V. 2005, ApJ, 635, 931
- Bullock, J. S., Kravtsov, A. V., & Weinberg, D. H. 2001, ApJ, 548, 33
- Busso, G., Moehler, S., Zoccali, M., Heber, U., & Yi, S. K. 2005, ApJ, 633, L29
- Catelan, M. 2009, Ap&SS, 320, 261
- Collins, M. L. M., et al. 2011, MNRAS, 413, 1548
- Cooper, A. P., et al. 2010, MNRAS, 406, 744
- Courteau, S., Widrow, L. M., McDonald, M., Guhathakurta, P., Gilbert, K. M., Zhu, Y., Beaton, R. L., & Majewski, S. R. 2011, ApJ, 739, 20
- Dalcanton, J. J., et al. 2012, ApJS, 200, 18
- Deason, A. J., Belokurov, V., & Evans, N. W. 2011, MNRAS, 416, 2903
- Dolphin, A. E. 2000, PASP, 112, 1383
- Dorman, C. E., et al. 2012, ApJ, 752, 147
- Dotter, A., et al. 2010, ApJ, 708, 698
- Durrell, P. R., Harris, W. E., & Pritchett, C. J. 1994, AJ, 108, 2114
- Durrell, P. R., Harris, W. E., & Pritchett, C. J. 2001, AJ, 121, 2557

- Durrell, P. R., Harris, W. E., & Pritchett, C. J. 2004, *AJ*, 128, 260
- Eggen, O. J., Lynden-Bell, D., & Sandage, A. R. 1962, *ApJ*, 136, 748
- Fan, Z., Ma, J., de Grijs, R., & Zhou, X. 2008, *MNRAS*, 385, 1973
- Flynn, C., Holmberg, J., Portinari, L., Fuchs, B., & Jahreiß, H. 2006, *MNRAS*, 372, 1149
- Font, A. S., McCarthy, I. G., Crain, R. A., Theun s, T., Schaye, J., Wiersma, R. P. C., & Dalla Vecchia, C. 2011, *MNRAS*, 416, 2802
- Gilbert, K. M., et al. 2007, *ApJ*, 668, 245
- Gilbert, K. M., Font, A. S., Johnston, K. V., & Guhathakurta, P. 2009a, *ApJ*, 701, 776
- Gilbert, K. M., et al. 2009b, *ApJ*, 705, 1275
- Gratton, R. G., Lucatello, S., Bragaglia, A., Carretta, E., Momany, Y., Pancino, E., & Valenti, E. 2006, *A&A*, 455, 271
- Guhathakurta, P., Ostheimer, J. C., Gilbert, K. M., Rich, R. M., Majewski, S. R., Kalirai, J. S., Reitzel, D. B., & Patterson, R. J. 2005, *ArXiv: astro-ph/0502366*
- Harris, W. E. 1996, *AJ*, 112, 1487
- Ibata, R., Chapman, S., Ferguson, A. M. N., Lewis, G., Irwin, M., & Tanvir, N. 2005, *ApJ*, 634, 287
- Ibata, R., Irwin, M., Lewis, G., Ferguson, A. M. N., & Tanvir, N. 2001, *Nature*, 412, 49
- Ibata, R., Martin, N. F., Irwin, M., Chapman, S., Ferguson, A. M. N., Lewis, G. F., & McConnachie, A. W. 2007, *ApJ*, 671, 1591
- Ibata, R. A., Gilmore, G., & Irwin, M. J. 1994, *Nature*, 370, 194
- Ibata, R. A., Gilmore, G., & Irwin, M. J. 1995, *MNRAS*, 277, 781
- Irwin, M. J., Ferguson, A. M. N., Ibata, R. A., Lewis, G. F., & Tanvir, N. R. 2005, *ApJ*, 628, L105
- Jurić, M., et al. 2008, *ApJ*, 673, 864
- Kalirai, J. S., Bergeron, P., Hansen, B. M. S., Kelson, D. D., Reitzel, D. B., Rich, R. M., & Richer, H. B. 2007, *ApJ*, 671, 748
- Kalirai, J. S., et al. 2006, *ApJ*, 648, 389
- Kazantzidis, S., Bullock, J. S., Zentner, A. R., Kravtsov, A. V., & Moustakas, L. A. 2008, *ApJ*, 688, 254
- Kinman, T. D., Morrison, H. L., & Brown, W. R. 2009, *AJ*, 137, 3198
- Layden, A. C. 1995, *AJ*, 110, 2312
- Majewski, S. R., Skrutskie, M. F., Weinberg, M. D., & Ostheimer, J. C. 2003, *ApJ*, 599, 1082
- Malin, D., & Hadley, B. 1999, in *Astronomical Society of the Pacific Conference Series*, Vol. 182, *Galaxy Dynamics - A Rutgers Symposium*, ed. D. R. Merritt, M. Valluri, & J. A. Sellwood, 445
- Martínez-Delgado, D., et al. 2010, *AJ*, 140, 962
- Martínez-Delgado, D., Peñarrubia, J., Gabany, R. J., Trujillo, I., Majewski, S. R., & Pohlen, M. 2008, *ApJ*, 689, 184
- McConnachie, A. W., et al. 2009, *Nature*, 461, 66
- Munshi, F., et al. 2012, *arXiv:1209.1389*
- O'Connell, R. W. 1999, *ARA&A*, 37, 603
- Pietrukowicz, P., et al. 2012, *ApJ*, 750, 169
- Preston, G. W., Shectman, S. A., & Beers, T. C. 1991, *ApJ*, 375, 121
- Radburn-Smith, D. J., et al. 2011, *ApJS*, 195, 18
- Rich, R. M., Corsi, C. E., Cacciari, C., Federici, L., Fusi Pecci, F., Djorgovski, S. G., & Freedman, W. L. 2005, *AJ*, 129, 2670
- Richardson, J. C., et al. 2008, *AJ*, 135, 1998
- Rosenfield, P., et al. 2012, *ArXiv: astro-ph/1206.4045*
- Saglia, R. P., et al. 2010, *A&A*, 509, A61
- Salaris, M., Riello, M., Cassisi, S., & Piotto, G. 2004, *A&A*, 420, 911
- Sarajedini, A., et al. 2007, *AJ*, 133, 1658
- Sarajedini, A., & Jablonka, P. 2005, *AJ*, 130, 1627
- Sarajedini, A., Yang, S.-C., Monachesi, A., Lauer, T. R., & Trager, S. C. 2012, *ArXiv: astro-ph/1206.6376*
- Schlegel, D. J., Finkbeiner, D. P., & Davis, M. 1998, *ApJ*, 500, 525
- Searle, L., & Zinn, R. 1978, *ApJ*, 225, 357
- Seigar, M. S., Barth, A. J., & Bullock, J. S. 2008, *MNRAS*, 389, 1911
- Siegel, M. H., Majewski, S. R., Reid, I. N., & Thompson, I. B. 2002, *ApJ*, 578, 151
- Stanek, K. Z., & Garnavich, P. M. 1998, *ApJ*, 503, L131
- Tanaka, M., Chiba, M., Komiyama, Y., Guhathakurta, P., Kalirai, J. S., & Iye, M. 2010, *ApJ*, 708, 1168
- Tanvir, N. R., et al. 2012, *MNRAS*, 422, 162
- van den Bergh, S. 1991, *PASP*, 103, 1053
- Watkins, L. L., Evans, N. W., & An, J. H. 2010, *MNRAS*, 406, 264
- Willman, B., et al. 2005, *ApJ*, 626, L85
- Worley, C. C., & Cottrell, P. L. 2010, *MNRAS*, 406, 2504
- Xue, X.-X., et al. 2011, *ApJ*, 738, 79
- Yanny, B., et al. 2000, *ApJ*, 540, 825
- Zolotov, A., Willman, B., Brooks, A. M., Governato, F., Brook, C. B., Hogg, D. W., Quinn, T., & Stinson, G. 2009, *ApJ*, 702, 1058

TABLE 1
 PROPERTIES OF THE M31 BLUE HORIZONTAL BRANCH

Field	R_{med} (kpc) ^a	$F814W_{BHB}$ ^b	N_{BHB} ^c	N_{RGB} ^d	F_{BHB} ^e
M31-B01-F07-WFC	1.64	...	<2000	25300	≤0.08
M31-B01-F13-WFC	1.70	...	<2300	20000	≤0.12
M31-B01-F01-WFC	1.70	...	<3100	30300	≤0.10
M31-B02-F11-WFC	2.47	...	<3400	10500	≤0.32
M31-B02-F04-WFC	2.96	...	<3100	8500	≤0.36
M31-B02-F16-WFC	2.95	25.233±0.018	1123±137	7240±85	0.16±0.01
M31-B02-F09-WFC	3.38	25.240±0.024	878±139	6048±78	0.15±0.01
M31-B02-F15-WFC	3.41	25.230±0.019	658±120	5276±73	0.12±0.01
M31-B02-F03-WFC	3.42	25.196±0.024	929±143	6473±80	0.14±0.01
M31-B02-F08-WFC	3.81	25.218±0.024	679±102	4279±65	0.16±0.01
M31-B02-F14-WFC	3.84	25.245±0.021	738±88	3652±60	0.2±0.01
M31-B02-F02-WFC	3.84	25.203±0.028	505±117	4865±70	0.1±0.01
M31-B02-F07-WFC	4.25	25.257±0.017	633±67	2965±54	0.21±0.01
M31-B02-F01-WFC	4.28	25.221±0.022	513±78	3395±58	0.15±0.01
M31-B02-F13-WFC	4.28	25.238±0.018	603±65	2614±51	0.23±0.01
B08 halo11	11.0	...	53±11	79±14	0.67±0.09
10394_M31-HALO-NW	17.7	...	29±5	45±7	0.64±0.15
B08 stream	20.2	...	11±3	22±5	0.50±0.10
B08 halo21	21.0	...	14±4	20±4	0.70±0.24
11632_M31-HALO-SE	24.5	...	8±3	15±4	0.53±0.23
B08 halo35ab	35.0	...	4±2	9±3	0.44±0.27

^a The median galactocentric distance of the stars in the the region kpc.

^b The F814W magnitude of the BHB at $0.1 < F475W - F814W < 0.5$.

^c The number of BHB stars from $0.1 < F475W - F814W < 0.5$ or equivalent.

^d The number of RGB stars from $1.5 < F475W - F814W < 3.5$ and $22.0 < F814W < 22.5$ or equivalent.

^e Fraction of BHB/RGB stars.

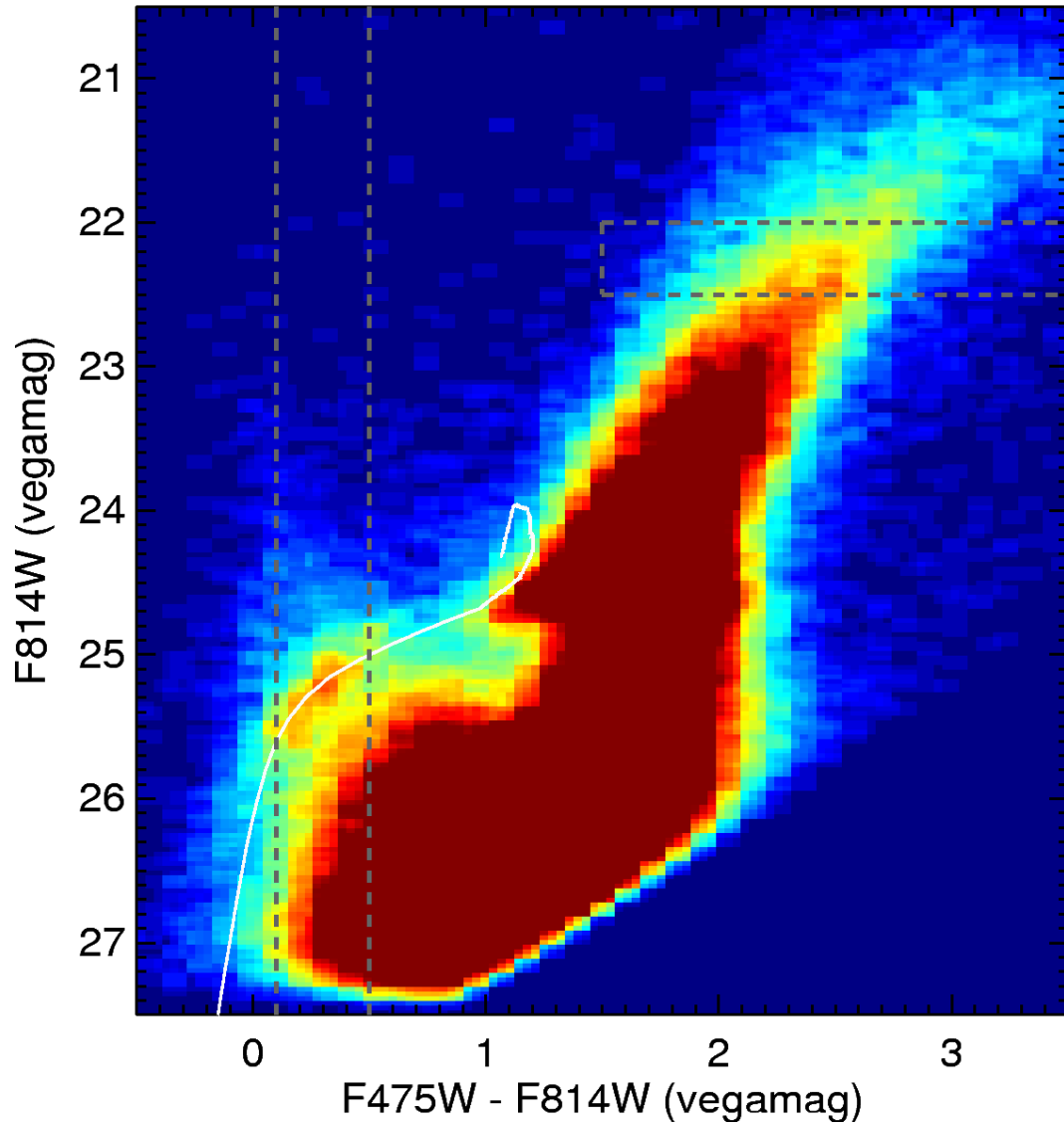


FIG. 1.— The color-magnitude diagram of the first PHAT field where we noticed the BHB ($R_{minor}=3.8$ kpc). Redder colors denote higher densities of data points. Overplotted in white is the theoretical zero age horizontal branch for $[\text{Fe}/\text{H}] = -1.7$ from the Padova stellar evolution models. The overdensity in the CMD associated with the BHB is clearly evident as the density peak coincident with the model at $F475W - F814W \sim 0.3$, $F814W \sim 25.3$. The metallicity has little effect in this sequence at the color of the BHB, but changes the shape of the red end. Overplotted in dashed gray lines are the boundaries over which we fit histograms in order to measure the properties of the BHB stars. The dashed gray box outlines the area in which we counted RGB stars for BHB/RGB ratios.

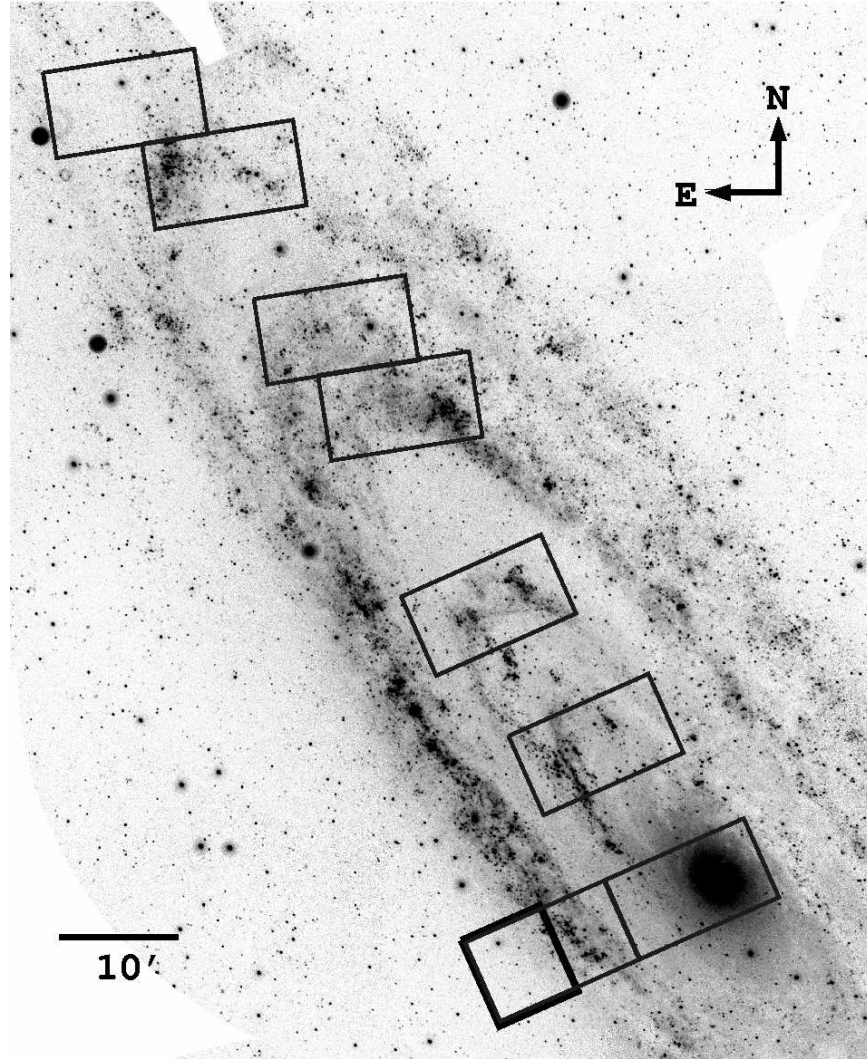


FIG. 2.— The northern half of the GALEX NUV image of M31. Thin line boxes show the regions of the PHAT survey completed when the BHB was seen. Thick black box shows the region where the BHB was noticed in the photometry: the area farthest out on the minor axis, with the lowest disk contribution.

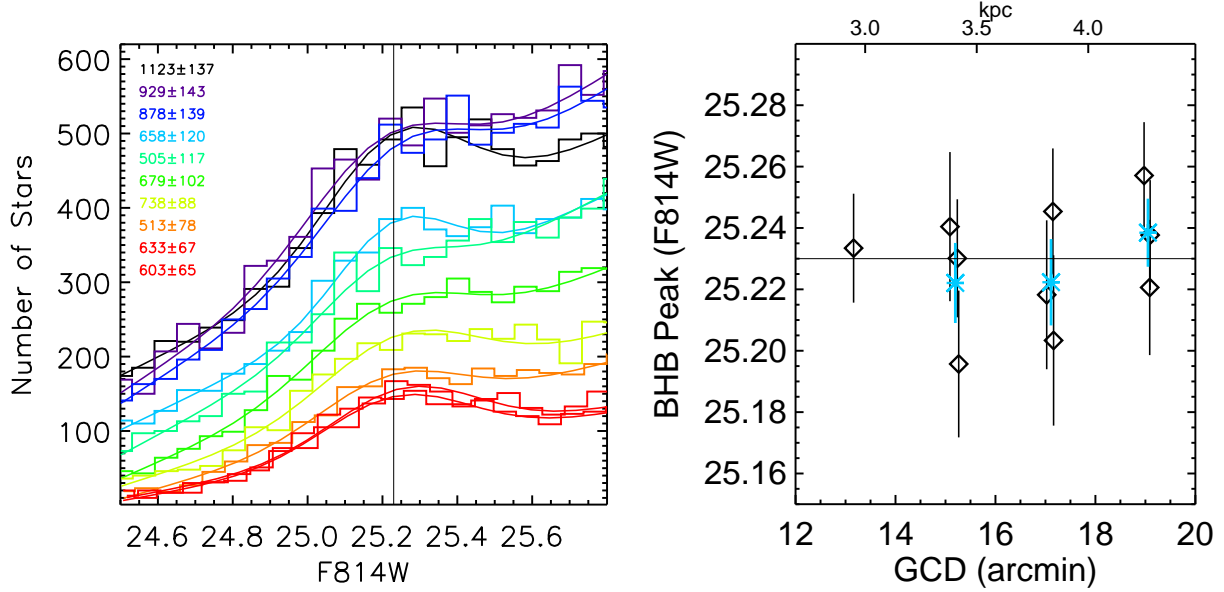


FIG. 3.— *Left*: Luminosity functions for stars with $0.1 < F_{475W} - F_{814W} < 0.5$, in PHAT fields with clear BHB features. Overplotted are the best-fitting line+Gaussian functions. Each field is represented by a different color. The numbers in the upper left indicate the number of stars (and uncertainty) in the Gaussian component. *Right*: The resulting best-fit apparent F814W magnitude for the center of the BHB as a function of galactocentric distance. Cyan points show the combined measurements of multiple fields at similar radii. There is no trend in BHB peak magnitude with radius or surface brightness in M31, thus the Gaussian fits are not significantly affected by crowding or completeness, and that the detected stars in each location are behind equal amounts of extinction. The BHB in M31 has $F_{814W} = 25.23$.

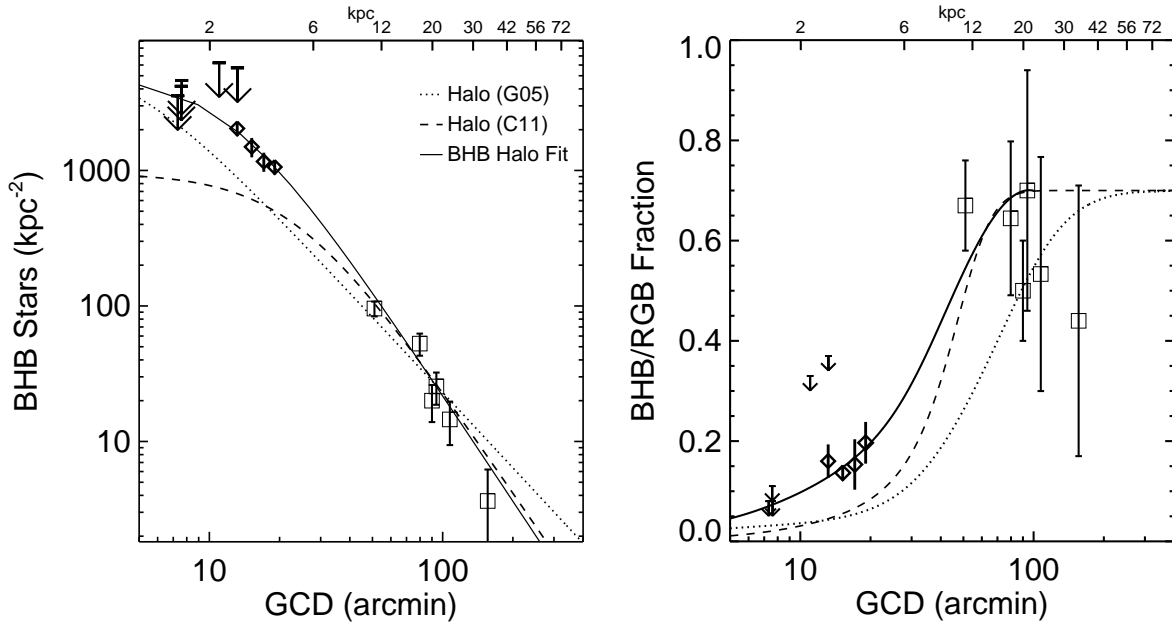


FIG. 4.— *Left*: The number density of BHB stars as a function of M31 galactocentric distance. Diamonds show combinations of the multiple measurements at similar radii in the PHAT data. Squares show the B08 and archival photometry. Upper-limits are shown with downward arrows. Dotted line: M31 halo profile from G05 normalized to match our data at 20 kpc. Dashed line: M31 halo profile from C11 normalized to match our data at 20 kpc. Solid line: a fit of the BHB data using the power-law halo parametrization of C11 ($\chi^2_{\nu} = 0.97$). *Right*: F_{BHB} as a function of galactocentric distance over the same radial range. Lines are from the same models as *Left* but represent $0.7 \times H/T$ where H is the Halo light and T is the total light in the two models. The low BHB/RGB ratios near the center are due to the bulge and disk components contributing substantially to the RGB but not to the BHB, and do not reflect metallicity changes in the halo component. The factor of 0.7 scales the fraction to the pure halo F_{BHB} value (see § 3.5). The curve corresponding to the BHB fit (solid curve) assumes the total from Guhathakurta et al. (2005) to compute fractions and is only computed out to the “pure halo” value (0.7) at 21 kpc.

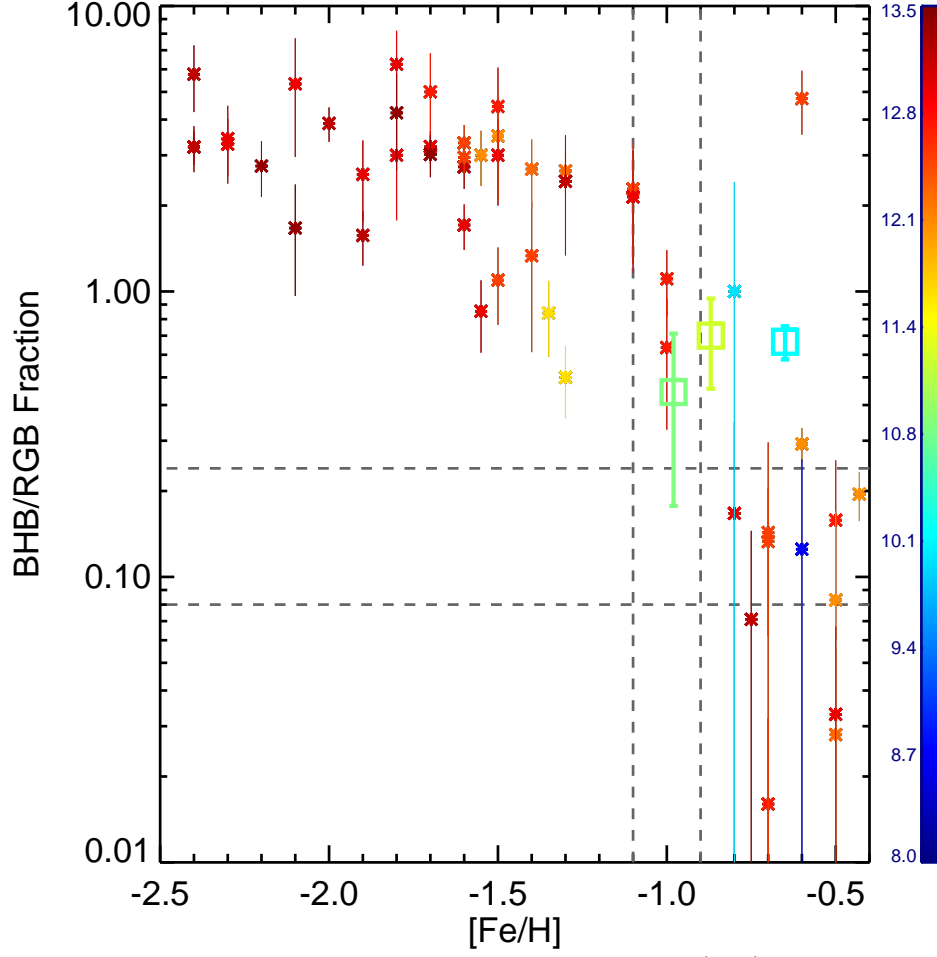


FIG. 5.— BHB fractions measured for Galactic GCs from the sample of Dotter et al. (2010) using the same CMD regions as for the M31 halo fields of B08. Points are color-coded by age, given by the color bar in Gyr. GCs are shown with asterisks. M31 points are shown with open squares using the ages and metallicities measured in B08. Dashed vertical lines mark the metallicity of the M31 thick disk (Collins et al. 2011). Dashed horizontal lines mark the range observed at 3–5 kpc from the galaxy center. We assume that the low values at these inner radii are in large part due to the disk and bulge components adding to the RGB, but not to the BHB.